



OPEN ACCESS

EDITED BY

Xiaohu Yang,
Xi'an Jiaotong University, China

REVIEWED BY

David Cabaleiro,
University of Vigo, Spain
Ana Moita,
University of Lisbon, Portugal

*CORRESPONDENCE

N. N. Liu,
✉ nannan.liu@irc.msu.ru

RECEIVED 28 March 2023

ACCEPTED 09 June 2023

PUBLISHED 07 July 2023

CITATION

Liu NN, Alekhina YA, Pyatakov AP, Zharkov MN, Yakobson DE, Pyataev NA, Sukhorukov GB, Perov NS and Tishin AM (2023), Impact of colloidal stabilization of MnZn-ferrite nanoparticles by oleic acid on their magnetothermal properties. *Front. Therm. Eng.* 3:1195740. doi: 10.3389/fther.2023.1195740

COPYRIGHT

© 2023 Liu, Alekhina, Pyatakov, Zharkov, Yakobson, Pyataev, Sukhorukov, Perov and Tishin. This is an open-access article distributed under the terms of the [Creative Commons Attribution License \(CC BY\)](https://creativecommons.org/licenses/by/4.0/). The use, distribution or reproduction in other forums is permitted, provided the original author(s) and the copyright owner(s) are credited and that the original publication in this journal is cited, in accordance with accepted academic practice. No use, distribution or reproduction is permitted which does not comply with these terms.

Impact of colloidal stabilization of MnZn-ferrite nanoparticles by oleic acid on their magnetothermal properties

N. N. Liu^{1*}, Yu. A. Alekhina¹, A. P. Pyatakov¹, M. N. Zharkov², D. E. Yakobson², N. A. Pyataev², G. B. Sukhorukov^{3,4}, N. S. Perov¹ and A. M. Tishin^{1,5}

¹Lomonosov Moscow State University, Moscow, Russia, ²National Research Ogarev Mordovia State University, Saransk, Russia, ³School of Engineering and Materials Science, Queen Mary University of London, London, United Kingdom, ⁴Skolkovo Institute of Science and Technology, Moscow, Russia, ⁵AMT&C Group, Troitsk, Russia

Introduction: The development of magnetic agents for magnetic fluid hyperthermia application is a complex task requiring simultaneous optimization of chemical, biomedical, magnetic, and, in particular, thermal properties of magnetic nanoparticles (MNPs). In the majority of papers, the magnetothermal measurements are carried out on bare MNPs suspended in deionized water with subsequent optimization of the required physiological and medical properties, including toxicity and biocompatibility. However, in real hyperthermia practice, the stable fluids or colloids of magnetic MNPs are used, and the colloidal stabilization can significantly modify their magnetic properties, including magnetothermal ones.

Methods: This paper is focused on the study of $Zn_xMn_{1-x}Fe_2O_4$ MNPs stabilized by oleic acid/sodium oleate in this context.

Results and Discussion: Our research demonstrates the crucial changes in the magnetic properties and magnetothermal response of ZnMn ferrite MNPs after the colloidal stabilization: while bare MNPs demonstrate significant coercivity, nonzero remanent magnetization, and superquadratic dependence of heat generation on the magnetic field amplitude, the magnetic properties of colloidal ZnMn ferrite MNPs are typical for superparamagnetic ones and their magnetothermal response is described by a conventional quadratic dependence on magnetic field amplitude. Various factors such as size distribution, magnetic anisotropy, and interparticle dipole–dipole interaction are considered as the origins of such an impact on magnetic MNPs' properties.

KEYWORDS

magnetic hyperthermia, specific absorption rate, magnetic nanoparticles, colloidal MNPs, oleic acid

1 Introduction

Magnetic hyperthermia has been widely investigated in recent years as an advanced clinical method for cancer treatment (Tishin, 2022). Magnetic hyperthermia is now considered a general-purpose method by regulatory agencies (FDA, EMA—European Medical Association—equivalent to the FDA). Deeply located tumors that are impossible

to treat with the existing laser technology can be treated by magnetic hyperthermia. In addition, tumors with poorly developed blood networks can be treated with magnetic hyperthermia when chemotherapy is ineffective. Laboratory and clinical studies have shown that, in most cases, tumors stop growing and decay (Rytov et al., 2022).

On the one hand, the improvement of the efficiency of magnetic nanoparticles' (MNPs) magnetic energy conversion into thermal energy is the key factor of this technology, whose efficiency is quantified as the specific absorption rate (SAR) that increases with the amplitude and frequency of magnetic field (Vijayakanth and Chintagumpala, 2022; Pucci et al., 2022). On the other hand, some physiological and patient safety issues should be taken into account. In addition to the well-known Brezovich limit [the product of frequency and magnetic field should not exceed $5 \times 10^8 \text{ A}/(\text{m} \cdot \text{s})$] (Brezovich, 1988), for real clinical application, the stable nontoxic and biocompatible fluids or colloids of MNPs are needed. The other factors to be considered are the shape and size of the MNPs, whether they have a shell, the stability of the suspension, whether the protein is recognized, the viability of the cells, whether the MNPs can be eliminated through the kidneys, etc. (Asín et al., 2012; Sanz et al., 2017; Salimi et al., 2020; Herrero de la Parte et al., 2022; Włodarczyk et al., 2022). Thus, the magnetothermal properties of MNP colloids depend not only on the amplitude and frequency of alternating magnetic fields but also on a number of physical–chemical characteristics, including those related to the technology of preparation of colloids of MNPs as well as physiological properties of cancer cells in Petri dish culture, mice tumor tissues, and eventually, human malignant neoplasms (Salimi et al., 2020). All aforementioned factors generally lead to the situation that the *in vitro* studies of MNPs in deionized water may not be directly applicable *in vivo* and need future additional investigations.

Scientists and radio engineers working in this field have to solve the magnetic hyperthermia trilemma (field–size–composition), which is similar to magnetic memory recording, but is much more complicated. For example, to make heating more efficient, it is necessary to optimize the SAR value while maintaining the product of frequency and amplitude within the Brezovich limit. In the case of superquadratic dependence of SAR on magnetic field amplitude, it enables reducing the operating frequencies to avoid technical difficulties with high-frequency source production. A decrease in field frequency leads to an increase in the optimal value of the relaxation time (satisfying the condition $2\pi\tau = 1$) and implies modification of size distribution and the anisotropy constant of the MNP. In magnetic memory media, to increase magnetic anisotropy, Co and Cr are widely used, but magnetic hyperthermia is restricted in the choice of materials: toxic Co and Cr cannot be used here.

Achieving optimal heat distribution in magnetic hyperthermia has also been investigated by (Rytov et al., 2022). For example, the advantages of using spherical magnetic nanocapsule assemblies composed of metallic iron MNPs covered with a non-magnetic shell of sufficient thickness in magnetic hyperthermia was demonstrated. Based on numerical simulations, the size and geometry of the biocompatible spherical capsules were optimized to minimize the effects of strong magnetic dipole interactions between closely spaced MNPs. Under alternating magnetic fields of moderate amplitude $H_0 = 50\text{--}100 \text{ Oe}$ and frequency $f = 100\text{--}200 \text{ kHz}$, the assembly of capsules can provide sufficiently high SAR values of

the order of 250–400 W/g for usage in clinical practice (Rytov et al., 2022).

In our previous papers (Liu et al., 2022a; Liu et al., 2022b; Liu et al., 2022c), the extensive studies of various factors affecting the SAR value of bare $\text{Zn}_x\text{Mn}_{1-x}\text{Fe}_2\text{O}_4$ MNPs suspended in deionized water were carried out within the aforementioned optimal magnetic field amplitude and frequency range ($H = 50\text{--}100 \text{ Oe}$, $f = 100\text{--}200 \text{ kHz}$). The superquadratic, up to 5th power, dependence on amplitude was observed for medium-sized MNPs (13–17 nm). This unusual property enables one to reduce the operating frequency to values more suitable for clinical application and to reduce the economic cost of the instrument (Liu et al., 2022a; Liu et al., 2022b; Liu et al., 2022c; Liu N. N. et al., 2022). Since the size of MnZn ferrite MNPs obtained by the co-precipitation method depends on Zn content, the optimum Zn concentration corresponding to the maximum SAR value at constant magnetic field amplitude shifts from 25% to 15% while the frequency decreases from 300 kHz to 100 kHz (Liu et al., 2022b). The magnetothermal measurements of the MnZn ferrite MNP suspension in glycerol enabled ruling out the Brown mechanisms of heating while the dependence of coercivity on Zn content showed that for the average particle size larger than 13 nm, the hysteresis mechanism of heating dominates (Liu et al., 2022a). These studies raised the question of whether the small superparamagnetic MNPs (<10 nm) are the best choice for magnetic hyperthermia, as was widely believed before (Pucci et al., 2022).

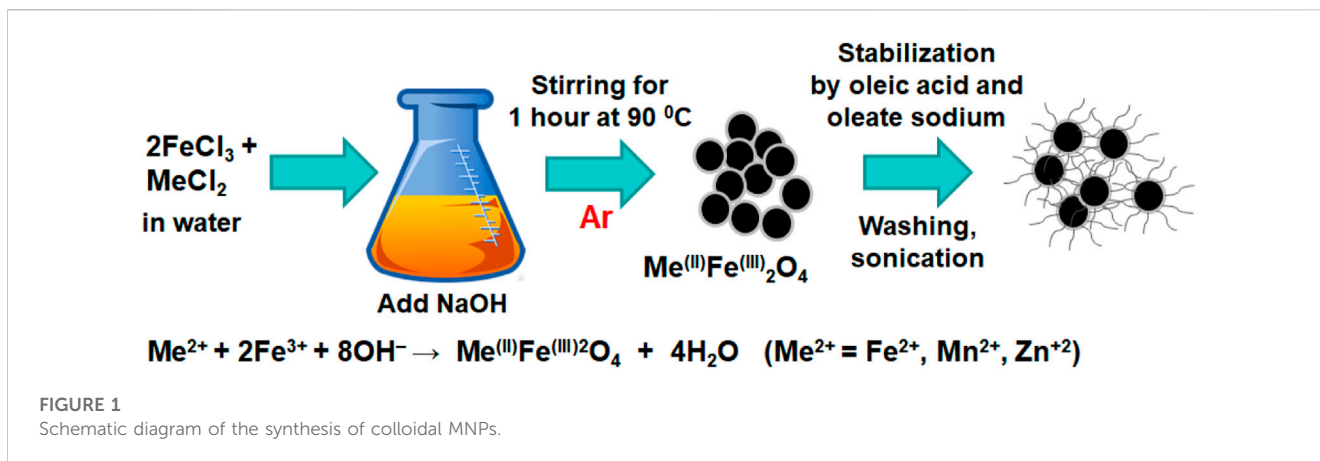
It should be noted, however, that the aforementioned results were obtained on bare MNPs while their clinical usage requires coating MNPs with the agent preventing opsonization of the MNPs introduced to an organism and their subsequent elimination by phagocytes. The colloidal stabilization of iron oxide MNPs with oleic acid/sodium oleate was shown to exert therapeutic effects for curing tumors via magnetic hyperthermia (Kulikov et al., 2022). Negligible toxicity, low local irritant effect, and no effect on the morphology of the internal organs were found. The efficiency of magnetic hyperthermia for the treatment of transplanted Walker 256 carcinoma with a survival rate of 85% was demonstrated in the studied therapy group of seven animals, while in the control group (without treatment), all animals died.

In this context, the magnetothermal properties of oleic acid/sodium oleate-coated MNPs are of special interest. The effect of colloidal stabilization on individual MNPs' magnetic and magnetothermal properties, as well as on the interparticle interaction, is insufficiently studied. This paper is focused on the comparison of SAR and the mechanisms of heating for coated and bare MNPs on the example of $\text{Zn}_x\text{Mn}_{1-x}\text{Fe}_2\text{O}_4$ ($x = 0,15$ and $0,2$) MNPs that were previously shown to have the largest SAR value (Liu et al., 2022a; Liu et al., 2022b; Liu et al., 2022c) in the prospective class of MnZn ferrite-based MNPs for hyperthermia application.

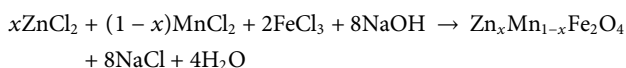
2 Material preparation and characterization

2.1 Magnetic nanoparticle synthesis

The schematic diagram of the synthesis of colloidal MNPs is presented in Figure 1. The process consists of two stages:



nanoparticle synthesis and stabilization. $Zn_xMn_{1-x}Fe_2O_4$ MNPs were obtained by co-precipitation of iron (III), manganese (II), and zinc salts from aqueous solutions in an alkaline environment of sodium hydroxide (Martins et al., 2022):



$MnCl_2 \cdot 4H_2O$, $ZnCl_2$ (in certain proportions), and $FeCl_3 \cdot 6H_2O$ (3.5 g) were dissolved in 30 mL of deionized water preheated to 90°C. Then, 20 mL of aqueous NaOH (2.5 g) was added rapidly to the solution with vigorous stirring. The resulting ferrite particle suspension was stirred for a further 1 h at a temperature of 90°C and then purified by magnetic decantation and washed 10 times with deionized water and ethanol at a volume ratio of 4:1. After every two washing procedures, the magnetic particles were sonicated (low-power ultrasonic bath) (35 kHz, 200 W) for 20 min.

The temperature and time of the ZnMn ferrite MNPs in this fabrication process are the same as those of the MNPs fabricated in our previous work (Liu et al., 2022b).

0.16 g NaOH was dissolved in a solution containing 2 mL deionized water and 3 mL ethanol. 1.75 mL of oleic acid was added to the basic solution, and the mixture was stirred. Thus, a solution containing sodium oleate and free oleic acid was obtained for the peptization and stabilization of purified particles.

A freshly prepared hydro-alcoholic solution of the stabilizer was added to the purified ferrite particle suspension, and the resulting suspension was vigorously stirred at 100°C for 1 h in a stream of argon. During the heat treatment, the ethanol evaporates. In the final stage, the suspension was centrifuged at 10,000 RPM for 10 min to remove large aggregates.

2.2 Size distribution and morphology

Transmission electron microscopy (TEM) measurements were performed on a high-resolution transmission electron microscope JEOL JEM-2010 to obtain the particle size distribution and MNP morphology. The particles have been re-suspended in ethanol and deposited on a copper mesh covered with a carbon film for examination in TEM (TEM images are presented in

Supplementary Figure SA1). For each type of MNPs, we collected 20 TEM images. These data were processed using Image-Pro Plus software.

It can be seen in Figure 2 that the size distribution of colloidal MNPs has been significantly changed compared with results for MNPs in deionized water. While the bare $Zn_xMn_{1-x}Fe_2O_4$ MNPs show a narrow distribution and a tendency for a mean size increase with an increase in Zn content (see the work of Liu et al. (2022b) for details), the colloidal MNPs for $x = 0.15$ and $x = 0.2$ have nearly the same mean value (14 and 15 nm, respectively) and wide size distribution with higher representation of small particles below 10 nm.

3 Magnetic measurements

Magnetic measurements were performed using a Lake Shore Model 7407 vibrating sample magnetometer (VSM) with a maximum magnetic field of 1.5 T and in the temperature range of 100 K–450 K.

The effective anisotropy constant according to Akulov's law of approximation to saturation (for bulk samples) (Akulov, 1931) is

$$\frac{\Delta M}{M_s} = \left(\frac{2aK}{HM_s} \right)^2, \quad (1)$$

where M is magnetization, H is the magnetic field, M_s is the saturation magnetization, K is magnetic anisotropy, and $a = 1/\sqrt{15}$ in the case of uniaxial anisotropy.

Taking into account the paraprocess, the tail of the hysteresis loop in the saturation region can be approximated with a linear function. The slope value is the coefficient b , and the intercept value is M_s . Approximation of the magnetization curve by this function will make it possible to obtain the values of the effective anisotropy constant:

$$K_{eff}^2 = -\frac{15}{4}H^2(M - M_s - bH)M_s. \quad (2)$$

The magnetization curve and hysteresis loop can be approximated by the Langevin function (taking into account the diamagnetic contribution):

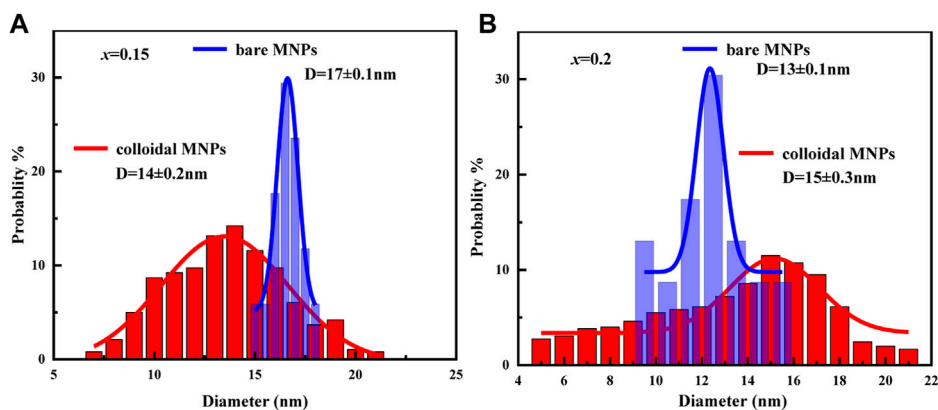


FIGURE 2

Histogram of the diameter distribution of $Zn_xMn_{1-x}Fe_2O_4$ ($x = 0.15, 0.2$) MNPs: (A) $x = 0.15$; (B) $x = 0.2$. The curve is fitted by the Gaussian distribution curve; red fitting curve: $Zn_xMn_{1-x}Fe_2O_4$ ($x = 0.15, 0.2$) colloidal MNPs; and blue fitting curve: $Zn_xMn_{1-x}Fe_2O_4$ ($x = 0.15, 0.2$) bare MNPs. Adapted from Liu et al. (2022b)¹, with permission from Elsevier.

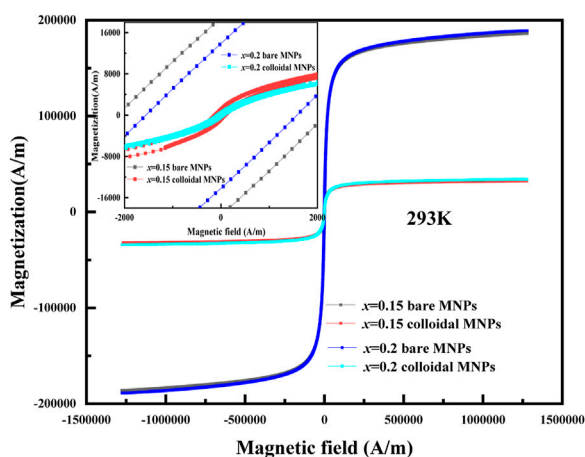


FIGURE 3

Hysteresis loops of $Zn_xMn_{1-x}Fe_2O_4$ ($x = 0.15, 0.2$) MNPs and colloidal MNPs at temperature $T = 293K$. The inset is an enlarged region of the hysteresis loop.

$$L(h) = P_1 \cdot \left(\text{cth}(P_2 \cdot (h - P_3)) - \frac{1}{P_2 \cdot (h - P_3)} \right) + P_4 \cdot h + P_5, \quad (3)$$

where h is a dimensionless magnetic field, P_1 , P_2 , P_3 , P_4 , and P_5 are selected parameters of the function: P_1 is saturation magnetization, P_2 is susceptibility, P_3 is coercivity, P_4 is linear contribution, and P_5 is the offset.

Figure 3 presents the hysteresis loops of $Zn_xMn_{1-x}Fe_2O_4$ ($x = 0.15, 0.2$) bare colloidal MNPs. The saturation magnetizations of

bare ZnMn ferrite MNPs suspended in ionized water are much higher than the saturation magnetization of colloidal MNPs. For bare MNPs, the magnetization for the $x = 0.2$ compound is somewhat higher than that for $x = 0.15$. On the contrary, for colloidal MNPs, the magnetization for the $x = 0.15$ compound is higher than that for the $x = 0.2$ one, and this tendency is even more pronounced at lower temperatures (See Supplementary Figure SA3; Supplementary Table S2).

Figure 4 presents typical hysteresis loops of $Zn_xMn_{1-x}Fe_2O_4$ ($x = 0.15, 0.2$) MNPs and colloidal MNPs at various amplitudes of a magnetic field. It can be seen that $M(H)$ curves of colloidal MNPs are typical for superparamagnetic MNPs (the coercivity of the hysteresis loops is below 400 A/m), while for bare MNPs, the coercivity is more than an order higher. The corresponding hysteresis loop area under the same magnetic field amplitude for bare MNPs is almost two orders of magnitude higher than for the colloidal MNPs (see Supplementary Figure SA4).

4 Magnetothermal measurement: specific absorption rate

To measure the magnetothermal properties of the MNPs, the AC magnetic field-calorimetry facility produced by the AMT&C Group (Moscow, Russia) has been used. A detailed description of the experimental conditions is given in our previous work (Liu et al., 2022b).

The specific absorption rate is calculated based on the temperature derivative with respect to time (Pérido et al., 2015; Pimentel et al., 2018):

$$SAR = C \left(\frac{dT}{dt} \right) \left(\frac{M}{m} \right), \quad (4)$$

where C is the heat capacity of the liquid, M/m is the ratio of the mass of water to the mass of MNPs, and dT/dt is the heating rate that can be obtained from the analysis of heating and cooling curves (see Supplementary Figure SA6; Supplementary Table S3) (Wilboer et al., 2014).

¹This article was published in J. Magnetism Magnetic Mater, 555, Liu, N. N., Pyatakov, A. P., Saletsky, A.M., Zharkov, M. N., Pyataev, N. A., Sukhorukov, G. B., The "field or frequency" dilemma in magnetic hyperthermia: The case of Zn-Mn ferrite nanoparticles, 169379, Copyright Elsevier (2022).

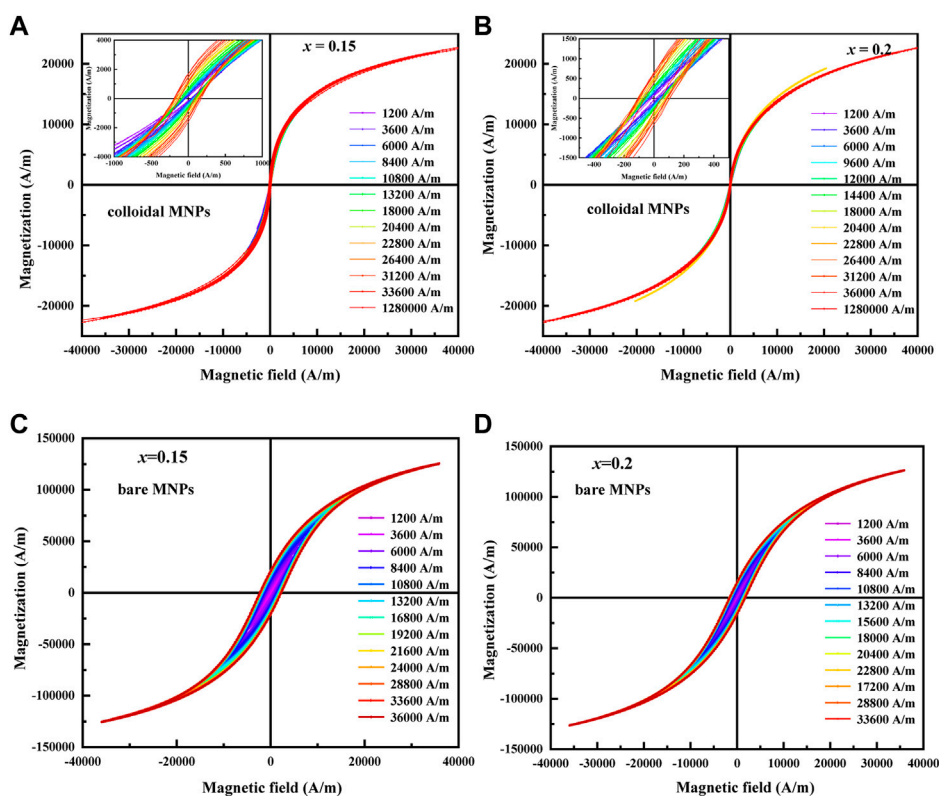


FIGURE 4

Hysteresis loops of $Zn_xMn_{1-x}Fe_2O_4$ bare and colloidal MNPs in different magnetic fields at temperature 300K. (A) $x = 0.15$, colloidal MNPs; (B) $x = 0.2$, colloidal MNPs; (C) $x = 0.15$, bare MNPs; and (D) $x = 0.2$, bare MNPs.

The SAR values measured at various frequencies and magnetic field amplitudes are shown in Figure 5. Quite surprisingly, the SAR values for colloidal MNPs are comparable with the ones for bare MNPs, despite the six times lower saturation magnetization and more than an order lower value of hysteresis loop area. To explain this counterintuitive fact, one needs to explore the mechanisms of heating of both bare MNPs and colloidal ones.

5 Discussion

To gain insight into the mechanisms of MNP heating, the field and frequency dependencies of SAR should be analyzed. It can be seen from Figure 5 that the magnetic field dependencies for the frequency range optimal for the hyperthermia procedure (~ 75 – 150 kHz) are different: the colloidal MNPs demonstrate conventional quadratic dependence on the amplitude of magnetic field typical for superparamagnetic particles, while for bare MNPs, this dependence is essentially superquadratic, up to 5th power. This striking difference can be attributed to the fundamentally different mechanisms of heating: for colloidal MNPs, the dominant mechanism is Néel relaxation proportional to the energy of magnetic field radiation ($\sim H^2$) (Rosensweig, 2002), while for bare MNPs, the major contribution is the hysteresis mechanism (Liu et al., 2022a; Liu et al., 2022b). This can be illustrated by Figure 6, which shows the comparison of experimental curves and the

calculated hysteresis contribution to the SAR obtained from the hysteresis loops areas of Figure 4. One can see that this contribution is negligible for colloidal MNPs (Figure 6A), while for bare MNPs, the effective SAR values calculated by hysteresis loops areas will reproduce the experimental dependence at field amplitude below 8000 A/m and gives the major contribution to the total SAR value in the practically relevant range of magnetic fields 6,000–12,000 A/m (Figure 6B).

The disappearance of highly superquadratic 5th power dependence on magnetic field amplitude in the case of colloidal MNPs may be attributed to the stability of colloidal MNPs in suspension, while bare MNPs in deionized water aggregates into large clusters with modified surface and bulk anisotropy of the particles and enhanced dipole–dipole interactions between them. Furthermore, the TEM data show that the particle size distribution for colloidal MNPs is wider (Figure 2), with a higher percentage of small particles in the colloid, and their shapes are irregular (Supplementary Figure SA1 in the Supplementary Material) compared to the almost circular shape of the bare ZnMn ferrite MNPs (Liu et al., 2022a; Liu et al., 2022b).

The presence of colloidal suspension MNPs with small volumes leads to the significant contribution of superparamagnetic MNPs with the dominant Néel relaxation mechanisms resulting in quadratic field dependence of the SAR on the magnetic field amplitude. Changes in the morphology of MNPs may also impact the values of shape and surface anisotropy of the MNPs in colloids.

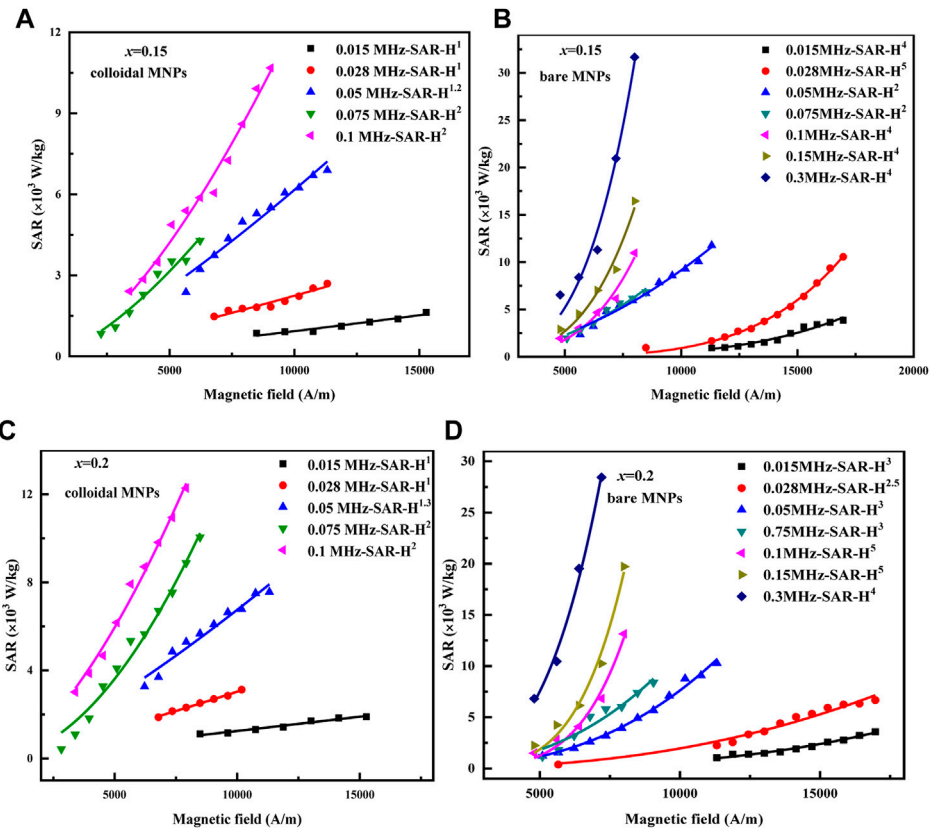


FIGURE 5 SAR values and curves for $Zn_xMn_{1-x}Fe_2O_4$ MNPs at various AC magnetic fields 2.4kA/m -16.7kA/m and at various frequencies 0.015–0.3 MHz. (A) $x = 0.15$, colloidal MNPs; (B) $x = 0.15$, bare MNPs in deionized water; (C) $x = 0.2$, colloidal MNPs; and (D) $x = 0.2$, bare MNPs in deionized water. Points correspond to the experimental values, and lines correspond to mathematical approximation by the method of least squares.

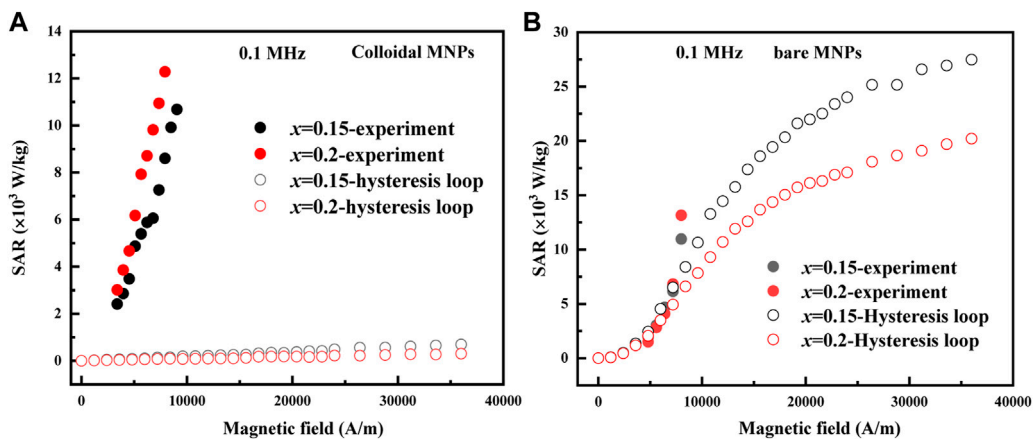
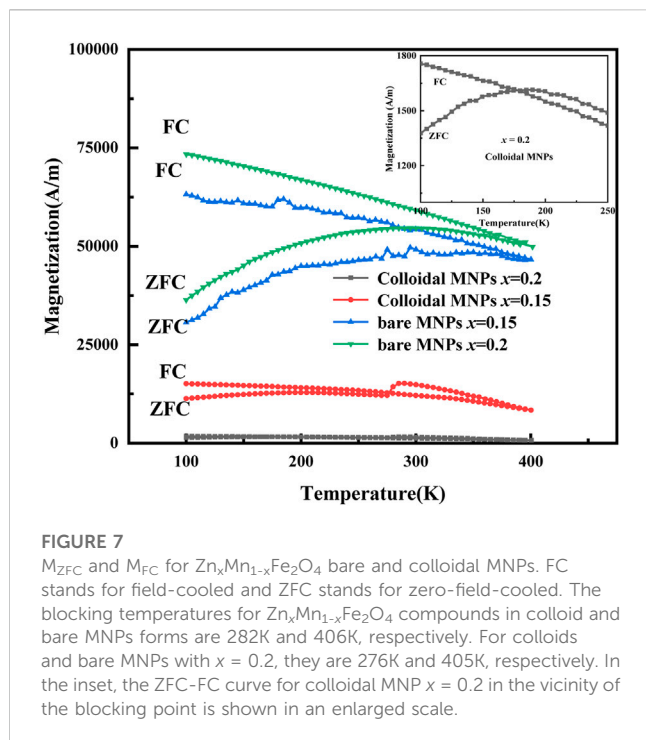


FIGURE 6 Hysteresis contribution to SAR values for $Zn_xMn_{1-x}Fe_2O_4$ ($x = 0.15, 0.2$) at various AC magnetic fields 0-40kA/m (0-500 Oe) and at frequencies 0.1 MHz: (A) colloidal MNPs and (B) bare MNPs. The operating frequency is 0.1 MHz.

To support the conclusion about the dominant role of superparamagnetism in the difference between the bare MNPs and the colloidal ones, we measure their blocking temperatures. The field-cooled and zero-field-cooled (ZFC-FC) curves for

$Zn_xMn_{1-x}Fe_2O_4$ ($x = 0.15, x = 0.2$) colloidal and bare MNPs are presented in Figure 7. The blocking temperatures for colloidal and bare MNPs differ drastically: about 280K and 405K, respectively.



Since the blocking temperature of colloids is significantly lower than that of bare MNPs, at room temperature, they behave like superparamagnetic particles with conventional magnetic field dependence of SAR, while bare MNPs at room temperature are in a blocked state, and the hysteresis mechanisms are relevant for them.

There were reports in the literature that the dipole-dipole interaction plays a crucial role in modifying the blocking temperature of MNPs; the stronger the interaction between MNPs, the higher the blocking temperature (Piñero-RedondoBañobre-López et al., 2011; Sadat et al., 2023). Consequently, the blocking temperature of $Zn_xMn_{1-x}Fe_2O_4$ ($x = 0.15$, $x = 0.2$) bare MNP systems with stronger dipolar interactions is substantially higher than that of the $Zn_xMn_{1-x}Fe_2O_4$ ($x = 0.15$, $x = 0.2$) colloid MNP systems. Thus, the dipole-dipole interaction can play a critical role in modifying the MNP relaxation mechanism.

To prove the hypothesis about the role of dipole-dipole interaction, we need to estimate and compare the strength of particle-to-particle interactions in bare MNPs and colloidal MNPs. A remanent map method based on the Stoner-Wohlfarth hysteresis model was applied (Mathews et al., 2021), including isothermal remanence (IRM) and direct current demagnetization (DCD) measurements (Figure 8). The IRM magnetization curves were obtained starting from the initial state (a freshly prepared sample not subjected to a magnetic field). A gradually increasing positive magnetic field is applied until H_{max} , and the residual magnetic m_{IRM} (H_{app}) is collected and then removed. The DCD curve is measured by saturating the sample in a negative field, $-H_{max}$, and then measuring the remanence m_{DCD} (H_{app}) after applying a reverse field up to H_{max} . The colloid particles show the zero value of remanent magnetization and negligible dipole-dipole interaction, while for bare ZnMn ferrite MNPs, it is significant.

It should be noted that even if all samples contained similar MNPs, the bare MNPs aggregation leads to an increased effective particle diameter, which will enhance interparticle interaction, increase the blocking temperature, and increase hysteresis loss. In contrast, the aggregation was much smaller in the colloid MNPs, resulting in a lower blocking temperature and lower hysteresis loss. Vargas et al. (2005) observed that for spherical magnetic MNPs with a narrow size distribution, by increasing the concentration, the interparticle spacing was shorter, resulting in higher blocking temperatures.

The influence of colloidal parameters on the SAR was especially discussed in the study by Piñero-RedondoBañobre-López et al. (2011) for another type of magnetic oxide (magnetite) MNPs. It was shown that at low particle concentrations, the coated magnetite particles can be considered the isolated ones, while for bare magnetite nanoparticles, significant interparticle interactions were present even at low particle concentrations. Furthermore, at higher concentrations, aggregation phenomena and cluster formation occurred (Piñero-RedondoBañobre-López et al., 2011). This observation agrees well with our conclusions derived from the analysis of data for ZnMn ferrite MNPs.

Finally, both in the model of Néel relaxation and hysteresis model, the energy losses during remagnetization are related to the magnetic anisotropy of an MNP. The magnetic anisotropy for all considered types of MNPs estimated in Akulov's law approximation of Eq. 2 is presented in Table 1. One can see that the anisotropy

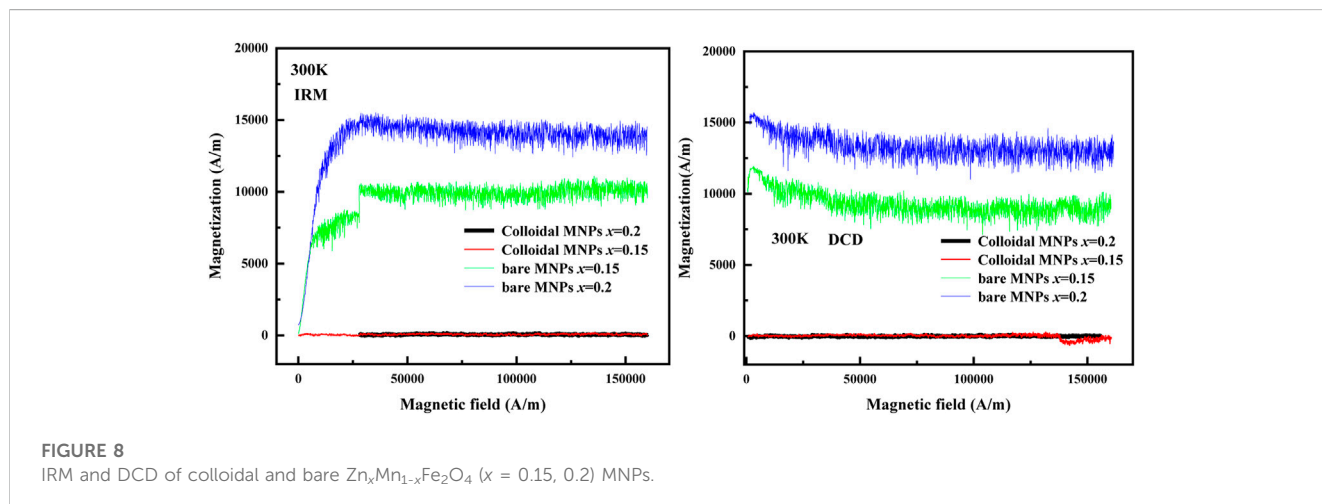


TABLE 1 Anisotropy constants of colloidal and bare $Zn_xMn_{1-x}Fe_2O_4$ ($x = 0.15, 0.2$) MNPs.

x	Anisotropy constant K ($\times 10^5$)
$x = 0.15$ colloidal MNPs	0.8 ± 0.1
$x = 0.2$ colloidal MNPs	0.7 ± 0.1
$x = 0.15$ bare MNPs	2.3 ± 0.3
$x = 0.2$ bare MNPs	2.3 ± 0.3

constants of colloidal MNPs are much smaller than those of bare MNPs. This fact also agrees with the superparamagnetic nature of colloidal MNPs.

6 Conclusion

Summarizing, the ZnMn ferrite MNPs were obtained by the chemical co-precipitation method and then stabilized with oleic acid/sodium oleate. The particle distribution, morphology, and magnetic and magnetothermal properties of bare and colloidal MNPs were compared. It was shown that in contrast to the bare MNPs demonstrating the dominant hysteresis mechanisms of heating (the significant coercivity, superquadratic dependence of SAR on magnetic field amplitude, nonzero remanent magnetization, etc.), the magnetothermal properties of colloidal ZnMn ferrite MNPs were typical for superparamagnetic ones: the negligibly small coercivity, zero remanent magnetization, and the conventional quadratic SAR dependence on magnetic field amplitude. It was shown that the superparamagnetic behavior of colloid MNPs and their low blocking point (below room temperature) can be attributed to a number of factors such as wider size distribution, low magnetic anisotropy, and negligible interparticle dipole–dipole interaction.

Data availability statement

The original contributions presented in the study are included in the article/[Supplementary Material](#); further inquiries can be directed to the corresponding author.

Author contributions

NL: methodology, data collection on magnetic hyperthermia and TEM, data analysis and interpretation, and article initial

drafting, writing, and final draft. YA: collection of magnetic data and the methodology of data processing. AP: conception and design of the work, methodology, data analysis and interpretation, final draft, and final approval of the version to be published. MZ: sample preparation and data collection. DY: sample preparation and data collection. NP: data analysis and interpretation and final approval of the version to be published. GS: conception and general support to the work, critical revision of the article, and final approval of the version to be published. NP: data interpretation and critical revision of the final text. AT: conception of the work, data analysis and interpretation, critical revision of the article, and final approval of the version to be published. All authors contributed to the article and approved the submitted version.

Funding

This work was supported by the Russian Foundation for Basic Research (grant number 19-29-10013). NL acknowledges the China Scholarship Council for study support.

Conflict of interest

Author AT was employed by company AMT&C Group.

The remaining authors declare that the research was conducted in the absence of any commercial or financial relationships that could be construed as a potential conflict of interest.

The author AT declares that they were an editorial board member of *Frontiers*, at the time of submission. This had no impact on the peer review process and the final decision.

Publisher's note

All claims expressed in this article are solely those of the authors and do not necessarily represent those of their affiliated organizations, or those of the publisher, the editors, and the reviewers. Any product that may be evaluated in this article, or claim that may be made by its manufacturer, is not guaranteed or endorsed by the publisher.

Supplementary material

The Supplementary Material for this article can be found online at: <https://www.frontiersin.org/articles/10.3389/ftther.2023.1195740/full#supplementary-material>

References

- Akulov, N. S. (1931). Über den verlauf der Magnetisierungskurve in starken feldern. *Z Phys.* 69, 822–831. doi:10.1007/BF01339465
- Asin, L., Ibarra, M. R., Tres, A., and Goya, G. F. (2012). Controlled cell death by magnetic hyperthermia: Effects of exposure time, field amplitude, and nanoparticle concentration. *Pharm. Res.* 29, 1319–1327. doi:10.1007/s11095-012-0710-z
- Brezovich, I. A. (1988). Low frequency hyperthermia: Capacitive and ferromagnetic thermoseed methods. *Med. Phys. Monogr.* Available at: https://scholar.google.com/hk/scholar?q=Low+frequency+hyperthermia:+Capacitive+and+ferromagnetic+thermoseed+methods&hl=zh-CN&as_sdt=0,5 16, 82–111.
- Herrero de la Parte, B., Rodrigo, I., Gutiérrez-Basoa, J., Iturrizaga Correcher, S., Mar Medina, C., Echevarria-Uraga, J. J., et al. (2022). Proposal of new safety limits for *in vivo* experiments of magnetic hyperthermia antitumor therapy. *Cancers* 14, 3084. doi:10.3390/cancers14133084
- Kulikov, O. A., Zharkov, M. N., Ageev, V. P., Yakobson, D. E., Shlyapkina, V. I., Zaborovskiy, A. V., et al. (2022). Magnetic hyperthermia nanoarchitectonics via

iron oxide nanoparticles stabilised by oleic acid: Anti-tumour efficiency and safety evaluation in animals with transplanted carcinoma. *IJMS* 23, 4234. doi:10.3390/ijms23084234

Liu, N. N., Pyatakov, A. P., Saletsky, A. M., Zharkov, M. N., Pyataev, N. A., Sukhorukov, G. B., et al. (2022b). The “field or frequency” dilemma in magnetic hyperthermia: The case of Zn Mn ferrite nanoparticles. *J. Magnetism Magnetic Mater.* 555, 169379. doi:10.1016/j.jmmm.2022.169379

Liu, N. N., Pyatakov, A. P., Zharkov, M. N., Pyataev, N. A., Cherepanova, J. V., Ichiyanagi, Y., et al. (2022c). The dependence of the magnetothermal properties of $Zn_xMn_{1-x}Fe_2O_4$ nanoparticles on the magnetic field near physiological Brezovich limit. *Phys. Met. Metallogr.* 123, 954–962. doi:10.1134/S0031918X22600919

Liu, N. N., Pyatakov, A. P., Zharkov, M. N., Pyataev, N. A., Sukhorukov, G. B., Alekhina, Y. A., et al. (2022a). Optimization of Zn–Mn ferrite nanoparticles for low frequency hyperthermia: Exploiting the potential of superquadratic field dependence of magnetothermal response. *Appl. Phys. Lett.* 120, 102403. doi:10.1063/5.0082857

Liu, N. N., Alekhina, Y. A., Pyatakov, A. P., Zharkov, M. N., Pyataev, N. A., Perov, N. S., et al. (2022d). Correlation of magnetic and magnetothermal properties of ZnMn ferrite nanoparticles. *Journals of Faculty of Physics Lomonosov Moscow State University*, 2241703.

Martins, F. H., Pilati, V., Paula, F. L. O., Gomes, R. C., Perzynski, R., and Depeyrot, J. (2022). Lattice strain of Zn–Mn mixed ferrite nanocrystals in a core-shell morphochemical structure. *Mat. Res.* 25, e20210596. doi:10.1590/1980-5373-mr-2021-0596

Mathews, S. A., Ehrlich, A. C., and Charipar, N. A. (2021). Author correction: Hysteresis branch crossing and the stoner–wohlfarth model. *Sci. Rep.* 11, 2891. doi:10.1038/s41598-021-81864-7

Pérido, E. A., Hemery, G., Sandre, O., Ortega, D., Garaio, E., Plazaola, F., et al. (2015). Fundamentals and advances in magnetic hyperthermia. *Appl. Phys. Rev.* 2, 041302. doi:10.1063/1.4935688

Pimentel, B., Caraballo-Vivas, R. J., Checca, N. R., Zverev, V. I., Salakhova, R. T., Makarova, L. A., et al. (2018). Threshold heating temperature for magnetic hyperthermia: Controlling the heat exchange with the blocking temperature of magnetic nanoparticles. *J. Solid State Chem.* 260, 34–38. doi:10.1016/j.jssc.2018.01.001

Piñero-RedondoBañobre-López, M., Pardiñas-Blanco, I., Goya, G., López-Quintela, M. A., and Rivas, J. (2011). The influence of colloidal parameters on the specific power absorption of PAA-coated magnetite nanoparticles. *Nanoscale Res. Lett.* 6, 383. doi:10.1186/1556-276x-6-383

Pucci, C., Degl’Innocenti, A., Belenli Gümüş, M., and Ciofani, G. (2022). Superparamagnetic iron oxide nanoparticles for magnetic hyperthermia: Recent advancements, molecular effects, and future directions in the omics era. *Biomater. Sci.* 10, 2103–2121. doi:10.1039/D1BM01963E

Rosensweig, R. E. (2002). Heating magnetic fluid with alternating magnetic field. *J. Magnetism Magnetic Mater.* 252, 370–374. doi:10.1016/S0304-8853(02)00706-0

Rytov, R. A., Bautin, V. A., and Usov, N. A. (2022). Towards optimal thermal distribution in magnetic hyperthermia. *Sci. Rep.* 12, 3023. doi:10.1038/s41598-022-07062-1

Sadat, M. E., Bud’ko, S. L., Ewing, R. C., Xu, H., Pauletti, G. M., Mast, D. B., et al. (2023). Effect of dipole interactions on blocking temperature and relaxation dynamics of superparamagnetic iron-oxide (Fe_3O_4) nanoparticle systems. *Materials* 16, 496. doi:10.3390/ma16020496

Salimi, M., Sarkar, S., Hashemi, M., and Saber, R. (2020). Treatment of breast cancer-bearing BALB/c mice with magnetic hyperthermia using dendrimer functionalized iron-oxide nanoparticles. *Nanomaterials* 10, 2310. doi:10.3390/nano10112310

Sanz, B., Calatayud, M. P., Torres, T. E., Fanarraga, M. L., Ibarra, M. R., and Goya, G. F. (2017). Magnetic hyperthermia enhances cell toxicity with respect to exogenous heating. *Biomaterials* 114, 62–70. doi:10.1016/j.biomaterials.2016.11.008

A. M. Tishin (Editor) (2022). *Magnetic materials and technologies for medical applications* (Duxford Cambridge, MA Kidlington, OX: WP: Woodhead Publishing, an imprint of Elsevier), 638.

Vargas, J. M., Nunes, W. C., Socolovsky, L. M., Knobel, M., and Zanchet, D. (2005). Effect of dipolar interaction observed in iron-based nanoparticles. *Phys. Rev. B* 72, 184428. doi:10.1103/PhysRevB.72.184428

Vijayakanth, V., and Chintagumpala, K. (2022). A review on an effect of dispersant type and medium viscosity on magnetic hyperthermia of nanoparticles. *Polym. Bull.* 80, 4737–4781. doi:10.1007/s00289-022-04324-w

Wildeboer, R. R., Southern, P., and Pankhurst, Q. A. (2014). On the reliable measurement of specific absorption rates and intrinsic loss parameters in magnetic hyperthermia materials. *J. Phys. D. Appl. Phys.* 47, 495003. doi:10.1088/0022-3727/47/49/495003

Włodarczyk, A., Gorgoń, S., Radoń, A., and Bajdak-Rusinek, K. (2022). Magnetite nanoparticles in magnetic hyperthermia and cancer therapies: Challenges and perspectives. *Nanomaterials* 12, 1807. doi:10.3390/nano12111807